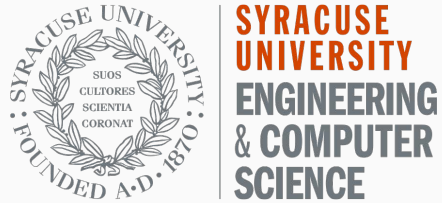

Disturbance observer-based data-driven control of unmanned aerial vehicles with uncertain dynamics

Amit K. Sanyal

NRI Project Kick-off Presentation
October 29, 2021
Syracuse, NY, USA

Department of Mechanical and Aerospace Engineering, Syracuse University

Introduction

Dynamics of UAVs in the Presence of Turbulent Air Flow

Unmanned aerial vehicles in the presence of turbulent air flow have uncertainties in their dynamics due to unknown and time-varying forces and moments induced by the turbulence.

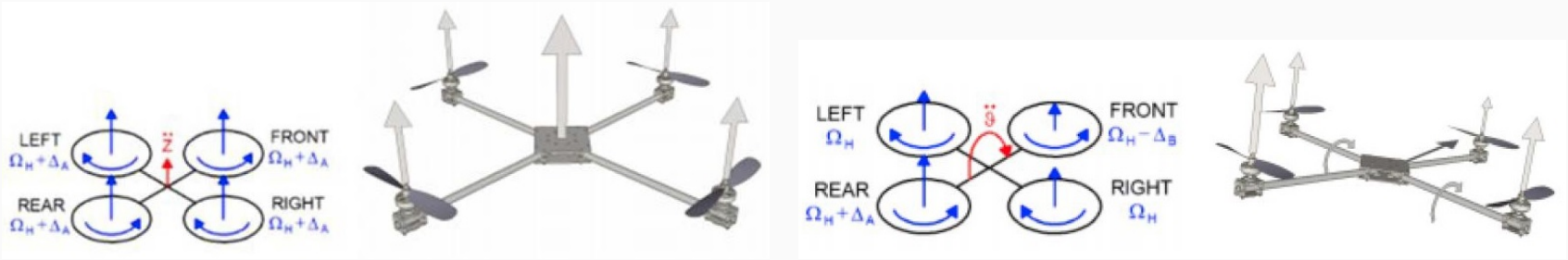

Figure 1: Vertical thrust and pitch forward created by rotors in a quadrotor UAV.

The usual configuration of multi-rotor UAVs has a fixed plane of rotors. This makes these UAVs under-actuated: with one degree of freedom in translation directly actuated by a body-fixed thrust direction perpendicular to the plane of rotors, and three degrees of freedom in attitude actuated by differential thrusts generated by the rotors.

Unknown Consequences of Turbulence on UAV Dynamics

Unsteady, turbulent air flow may change the differential thrusts created by rotors in multi-rotor UAVs for vertical thrust, pitch/roll, and yaw motions. This causes unknown but real effects on the dynamics of UAVs in the presence of turbulence. These effects include:

- Possible loss of lift resulting in large vertical translations that may lead to, e.g., UAV hitting the ground
- Large changes in torque resulting in large attitude changes
  - Adverse effects on stability of platform
- Autopilots may stiffen attitude response locally, which in turn could exacerbate the stability problem due to overshoot
  - Linear attitude control schemes (e.g., PID) based on yaw-pitch-roll angles have been observed to do this in experiments with quadrotor UAVs

Disturbance Observer-based Control

The basic approach for disturbance/uncertainty estimation-based control is shown in Fig. 4. The key points to note here are:

- The controller $C(z)$ can be designed according to tracking performance specifications and stability.
- Inner loop is designed to reject disturbance and suppress uncertainty.
- An ideal control system design is a balance between these conflicting requirements based on the application.

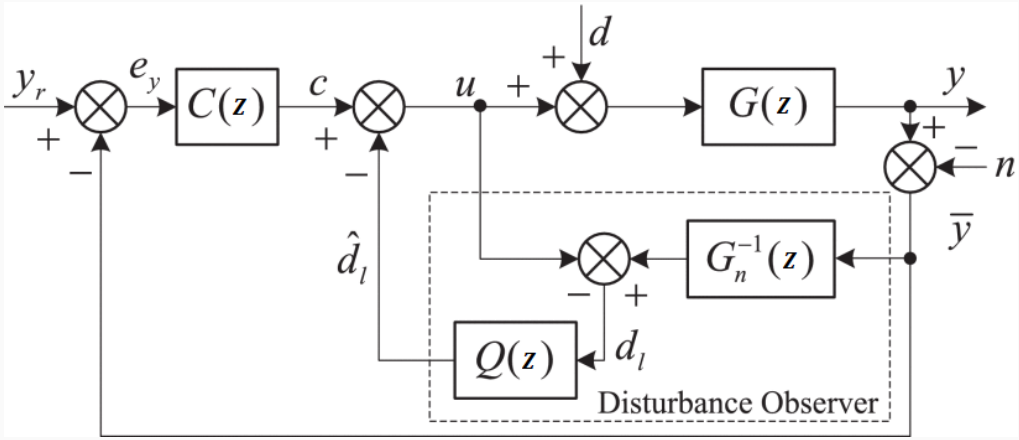

Figure 2: Conceptual diagram of disturbance-observer based control (DOBC).

Motivation:

- UAV flights over wildland fires are subject to unsteady and turbulent airflow.
- These effects create disturbance forces and torques that can adversely affect the control performance.
- Important to ensure nonlinearly stable and robust flight of the UAV in these circumstances.
  - Disturbance observer designs are useful in this regard.

Proposed DO design

- A finite-time stable disturbance observer (FTSDO) has faster convergence and better disturbance rejection than conventional DO designs.
- Systems that have a finite settling-time are more robust to bounded changes to system dynamics than asymptotically or exponentially stable systems.

Figure 3: UAV flight over wildfire

The Approach

Geometric Mechanics to Represent UAV Motions

We use the framework of geometric mechanics (GM) to represent (possibly large) rotational and translational motions of UAVs in 3D. This framework is advantageous because it addresses large, possibly unconstrained 3D motion without issues like *gimbal lock* encountered by other approaches.

Aerospace vehicles, including UAVs, have some amount of uncertainty in their flight dynamics due to external causes (e.g., atmospheric turbulence, drag, etc.,) and internal causes (e.g., changing mass, shifts in inertia, etc.). The resultant force and resultant torque caused by these uncertainties on the flight dynamics can be learnt "on the fly" using feedback from sensor data using a disturbance observer (DO).

Our technical approach for data-driven robust control of UAV in turbulent air flow above wildland fires would combine these two streams, GM and DO, into a seamless overall scheme. *This is the first time such a combined approach will be attempted, anticipating a new field of geometric data-driven control*.

Data-driven Control Approach

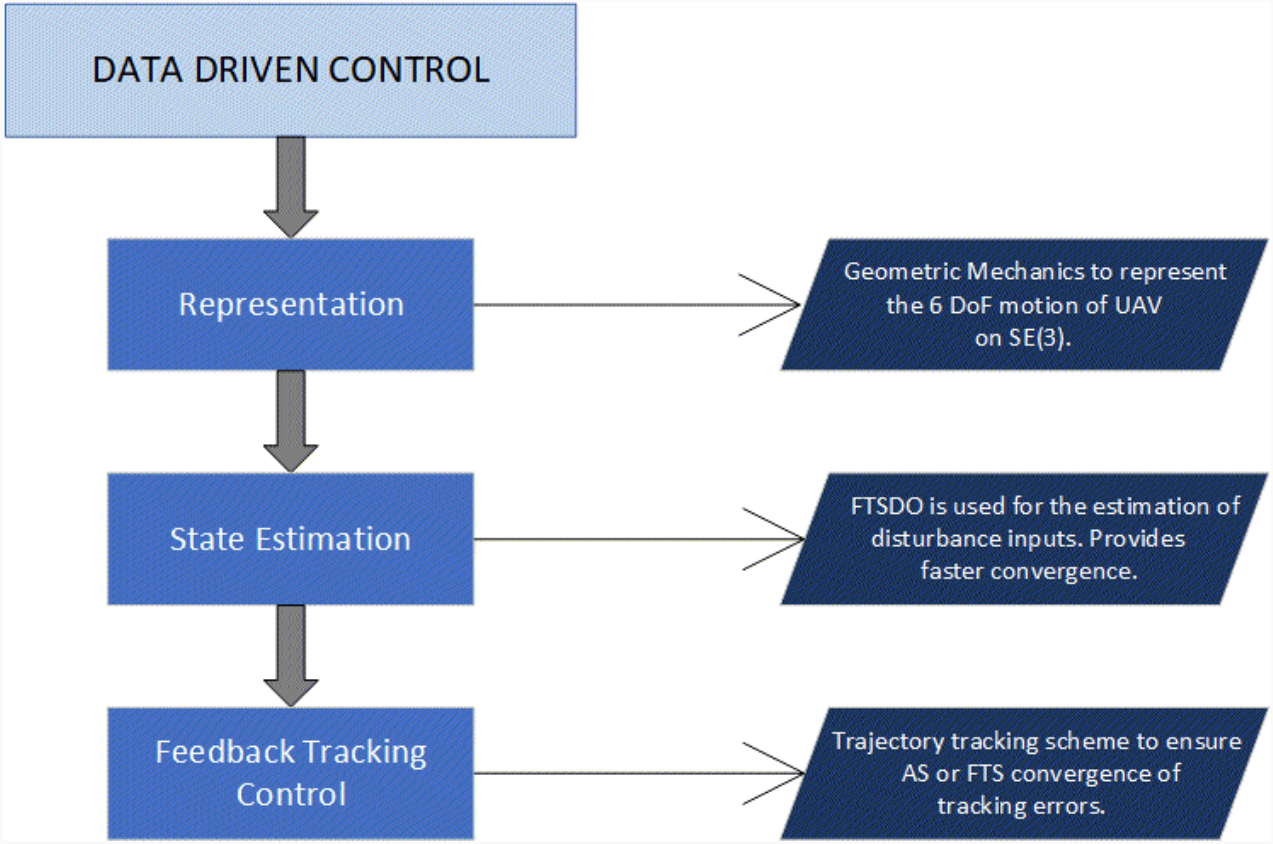

Figure 4: Overall approach for data-driven control of UAV in turbulent air flow.

Sequence of Frame Transformations

- A sequence of rotations and translations of a rigid body in (continuous or discrete) time is represented by a sequence of frame transformations between an inertial (spatial) coordinate frame and a body-fixed coordinate frame.
- The frame transformation at an instant also gives the instantaneous pose (position and orientation) of the rigid body.
- The group of rigid body frame transformations is a Lie group denoted $\mathrm{SE}(3)$. The total transformation in a discrete-time sequence is $g = g_1 \cdot g_2 \cdots g_n \in \mathrm{SE}(3)$.

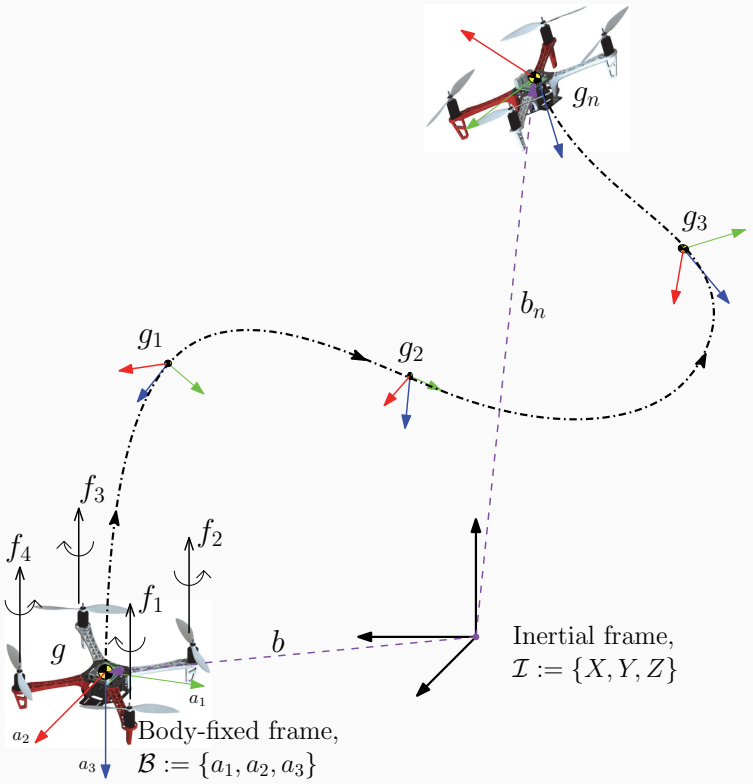

Figure 5: UAV flight as a sequence of frame transformations in time.

Representation of motion using GM

Pose of the UAV is given by the frame transformation

$$g = \begin{bmatrix} R & b \\ 0 & 1 \end{bmatrix} \in \mathrm{SE}(3), \tag{1}$$

- $b \in \mathbb{R}^3$: the position vector in an inertial frame $\mathcal{I}$,
- $R \in \mathrm{SO}(3)$: the rotation matrix from frame $\mathcal{B}$ to frame $\mathcal{I}$.

Kinematics of an UAV:

$$\begin{cases} \dot{b} = v = R\nu, \\ \dot{R} = R\Omega^{\times}, \end{cases} \tag{2}$$

- $v, \nu \in \mathbb{R}^3$: the velocity vector in inertial frame $\mathcal{I}$ and body-fixed frame $\mathcal{B}$, respectively.
- $\Omega \in \mathbb{R}^3$: the angular velocity in frame $\mathcal{B}$ and $\Omega^{\times}$ is the cross-product operator.

Dynamics of UAV with a body-fixed plane of rotors:

$$\begin{cases} m\ddot{b} = m\dot{v} = (f^c R - mg)e_3 + \phi_d, \\ J\dot{\Omega} = \tau^c - \Omega^{\times} J\Omega + \tau^d. \end{cases} \tag{3}$$

Discretized UAV dynamics using GM

Using the discrete Lagrange d'Alembert principle, the discretized equations of motion are:

$$\begin{cases} b_{k+1} = b_k + hR_k\nu_k, \\ R_{k+1} = R_k \exp\left(h\Omega_k^{\times}\right), \\ m\nu_{k+1} = hR_{k+1}^{\mathrm{T}}(f_k^c - mg)e_3 + h\varphi_k^d, \\ J\Omega_{k+1} = h\tau_k^c + exp(-h\Omega_k^{\times})J\Omega_k + h\tau_k^d, \end{cases} \tag{4}$$

where $\varphi_k^d = hR_{k+1}^{\mathrm{T}}\phi_k^d$.

These equations are obtained in the form of a Lie group variational integrator (LGVI). The matrix exponential in (4) is given by Rodrigues' rotation formula:

$$\exp\left(h\Omega^{\times}\right) = I + \frac{\sin\|h\Omega\|}{\|h\Omega\|}(h\Omega^{\times}) + \frac{1-\cos\|h\Omega\|}{\|h\Omega\|^2}(h\Omega^{\times})^2. \tag{5}$$

Problem Setup for Disturbance Observer Design

Given reasonably accurate estimates of the output and state variables are available, the estimation equations for displacement forces and torques are given by:

$$\begin{cases} \phi_k^d = \frac{1}{h}(m\hat{\nu}_{k+1} - h\hat{R}_{k+1}^T(f_k^c - mg)e_3), \\ \tau_k^d = \frac{1}{h}(J\hat{\Omega}_{k+1} - h\tau_k^c - exp(-h\Omega_k^\times)J\Omega_k). \end{cases} \tag{6}$$

The unknown disturbance inputs $\chi_k^d = (\Phi_k^d, \tau_k^d) \in \mathbb{R}^6$ are learnt in real time according to the past input-output history using (6). Let us denote the error in estimating χ_k as:

$$e_k^\chi := \hat{\chi}_k^d - \chi_k^d. \tag{7}$$

Also, the first order finite difference of the unknown dynamics, χ_k^d, is given by:

$$\Delta\chi_k := \chi_k^{(1)} = \chi_{k+1} - \chi_k \tag{8}$$

Preliminary work on a disturbance observer for $\hat{\chi}_k^d$ that is nonlinearly stable is described next.

Preliminary Results

Finite-time Stable Disturbance Observer in Discrete Time

A nonlinear observer for χ_k given by

$$\hat{\chi}^d_{k+1} = \mathcal{D}(e^\chi_k)e^\chi_k + \chi^d_k, \tag{9}$$

with given initial estimate $\hat{\chi}^d_0 = \chi^d_0$ and $\mathcal{D} : \mathbb{R}^+ \rightarrow R$ is a Hölder-continuous function that is designed to make this observer finite-time stable. This observer design leads to finite time stable convergence of the estimation error vector $e^\chi_k \in \mathbb{R}^6$ to a bounded neighborhood of $0 \in \mathbb{R}^6$, where bounds on the neighborhood are obtained from the bounds on $\Delta\chi_k$.

The Hölder-continuous function $\mathcal{D}(e^\chi_k)$ is given by:

$$\mathcal{D}(e^\chi_k) = \frac{((e^\chi_k)^T e^\chi_k)^{1-1/r} - \lambda}{((e^\chi_k)^T e^\chi_k)^{1-1/r} + \lambda}, \tag{10}$$

where $\lambda > 0$ and $r \in (1,2)$ are constants.

Boundedness of Disturbance Estimation Error

*Consider the nonlinear observer law for the disturbance χ_k given by (9). Let the bound on the first order difference $\Delta\chi_k$ defined by (9) be given by:

$$\|\Delta\chi_k\| \leq B^{\chi}, \tag{11}$$

*where $B_{\chi} \in \mathbb{R}^{+}$. Then, the observer estimation error e_k^{χ} is guaranteed to converge to the neighborhood given by:

$$N^{\chi} := \{e_k^{\chi} \in \mathbb{R}^n : \rho(e_k^{\chi})\|e_k^{\chi}\| \leq B^{\chi}\}, \tag{12}$$

*for finite $k > N$, $N \in \mathbb{W}$, where

$$\rho(e_k^{\chi}) := 1 + |\mathcal{D}(e_k^{\chi})|. \tag{13}$$

*Based on A. K. Sanyal, "Data-Driven Discrete-time Control with Hölder-Continuous Real-time Learning," *International Journal of Control*, 2021, doi: 10.1080/00207179.2021.1901993

Numerical Simulation Setup

A numerical simulation study for the FTS disturbance observer in slide 11 is carried out

- The turbulence is modeled as a combination of sinusoidal frequencies.
- Lower frequency signals of relatively higher amplitude are combined with higher frequency signals of relatively lower amplitudes, with the frequencies being not more than 10 Hz.
- The total magnitude of the force and torque disturbance is of the order of $\sim$5-7 N and $\sim$1-2 N-m, respectively.
- Output measurements are assumed at a constant rate of 50 Hz, i.e. sampling period $\Delta t = 0.02$ s.
- The first order finite-time stable observer stated in Theorem 1 is used for getting the disturbance estimate. The Hölder-continuous function $\mathcal{D}(e_k^\chi)$ defined in (10) is taken as:

$$\mathcal{D}(e_k^\chi) = \frac{((e_k^\chi)^T e_k^\chi)^{1-1/r} - \lambda}{((e_k^\chi)^T e_k^\chi)^{1-1/r} + \lambda}, \tag{14}$$

with $\lambda = 1.0$, and $r = \frac{9}{7}$.

Numerical Simulation Results

- The finite-time stability, robustness and bounds on the magnitude of disturbance terms are examined.
- Figure 6 shows the estimation error in the magnitude of disturbance force $\|e_k^{\Phi}\|$, and disturbance torques $\|e_k^{\tau}\|$, showing finite-time stability (FTS).
- Figure 7 shows the estimation errors in the presence of measurement noise which are taken to be ~ 2 % of the true output values which gives a realistic signal-to-noise ratio (SNR) around 30 dB.
- It can be clearly inferred from the plots that the disturbance estimation error settles down in the neighborhood of the zero vector in finite-time for relatively large initial disturbance estimation errors.
- The disturbance estimation errors from the FTS DO are found to satisfy the bounds given by the result in slide 12.

Simulation Results (without measurement noise)

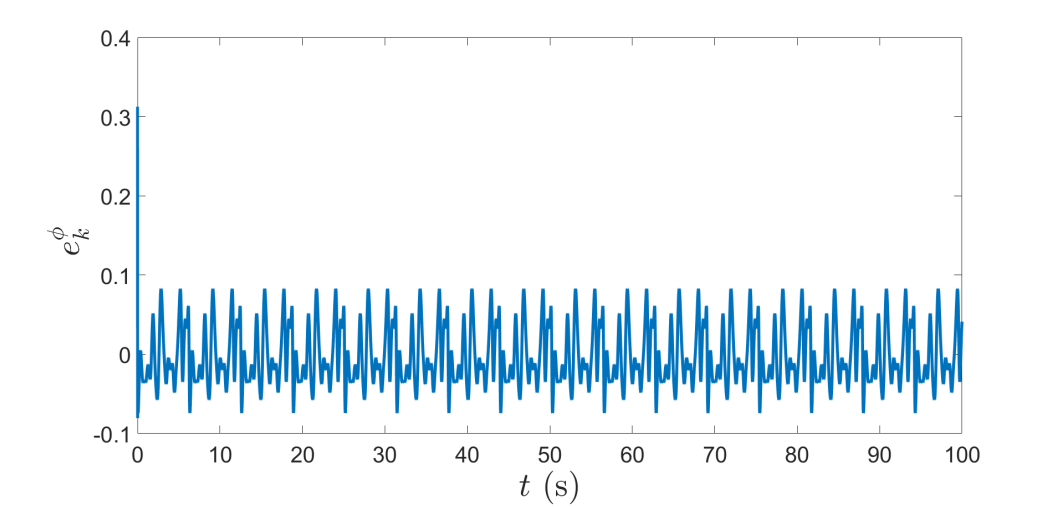

(a) Magnitude of estimation error for disturbance force

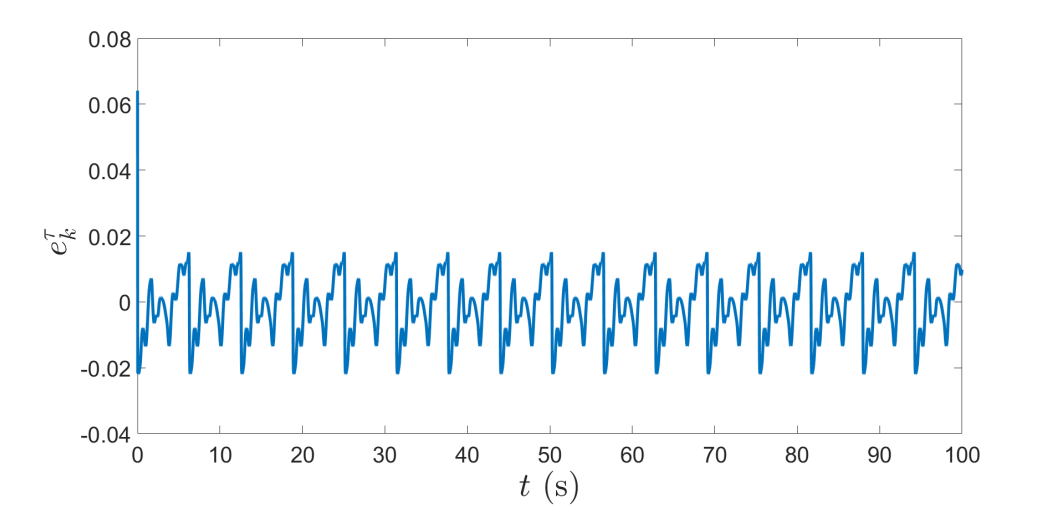

(b) Magnitude of estimation error for disturbance torque

Figure 6: Estimation error for disturbance inputs without measurement noise

Simulation Results (with measurement noise)

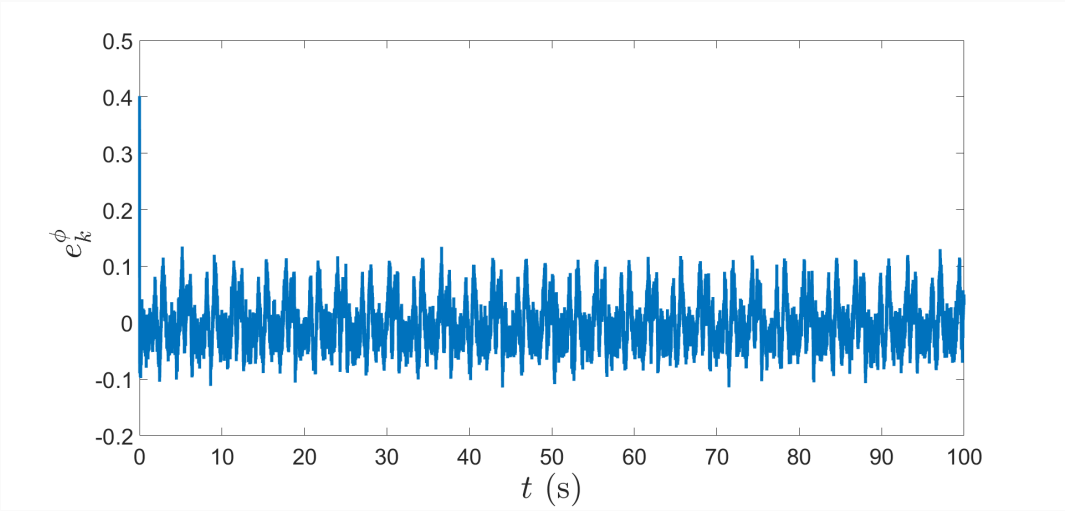

(a) Magnitude of estimation error for disturbance force

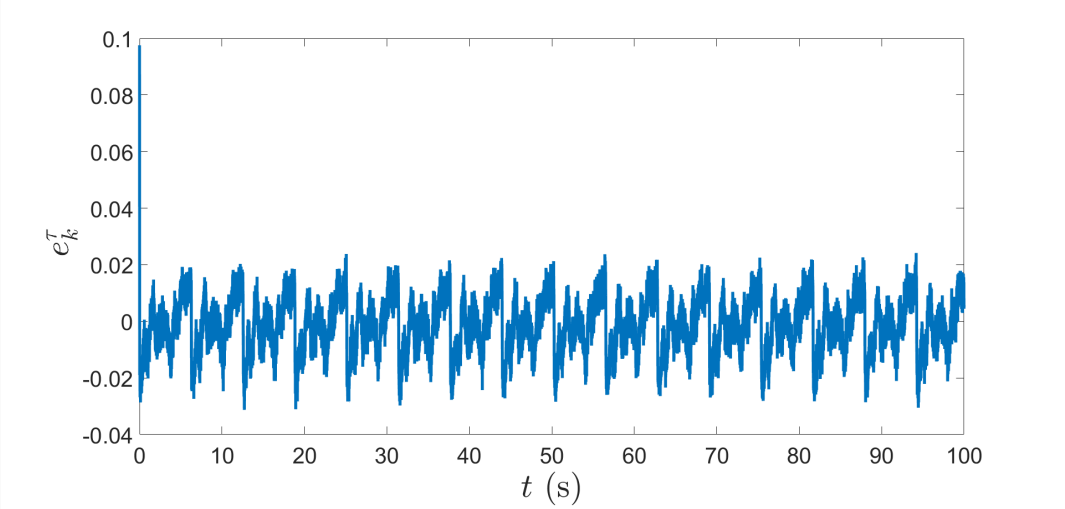

(b) Magnitude of estimation error for disturbance torque

Figure 7: Estimation error for disturbance inputs with noise

Next Steps

Continuing Work

- These preliminary results were submitted for peer review to the American Control Conference to be held in summer of 2023.
- Higher order FTS disturbance observer designs are also being developed.
- SITL testing of the FTS DO on ROS/Gazebo is being planned.

Acknowledgements

Award ID numbers 2132798/2132799